Journal of Assisted Reproduction and Genetics (2023) 40:491–508
https://doi.org/10.1007/s10815-023-02765-4

FERTILITY PRESERVATION

BNIP3-mediated autophagy via the mTOR/ULK1 pathway induces primordial follicle loss after ovarian tissue transplantation

Fengxia Liu[1] · **Mujun Li**[1,2]

Received: 26 October 2022 / Accepted: 23 February 2023 / Published online: 4 March 2023

Abstract

Purpose To explore the underlying mechanism of primordial follicle loss in the early period following ovarian tissue transplantation (OTT).

Methods BNIP3 was selected through bioinformatic protocols, as the hub gene related to autophagy during OTT. BNIP3 and autophagy in mice ovarian grafts and in hypoxia-mimicking KGN cells were detected using immunohistochemistry, transmission electron microscopy (TEM), western blotting, qPCR, and fluorescence staining. The regulatory role played by BNIP3 overexpression and the silencing of KGN cells in autophagy via the mTOR/ULK1 pathway was investigated.

Results Ultrastructure examination showed that autophagic vacuoles increased after mice ovarian auto-transplantation. The BNIP3 and autophagy-related proteins (Beclin-1, LC3B, and SQSTM1/p62) in mice ovarian granulosa cells of primordial follicle from ovarian grafts were altered compared with the control. Administration of an autophagy inhibitor in mice decreased the depletion of primordial follicles. In vitro experiments indicated that BNIP3 and autophagy activity were upregulated in KGN cells treated with cobalt chloride ($CoCl_2$). The overexpression of BNIP3 activated autophagy, whereas the silencing of BNIP3 suppressed it and reversed the autophagy induced by $CoCl_2$ in KGN cells. Western blotting analysis showed the inhibition of mTOR and activation of ULK1 in KGN cells treated with $CoCl_2$ and in the overexpression of BNIP3, and the opposite results following BNIP3 silencing. The activation of mTOR reversed the autophagy induced by BNIP3 overexpression.

Conclusions BNIP3-induced autophagy is crucial in primordial follicle loss during OTT procedure, and BNIP3 is a potential therapeutic target for primordial follicle loss after OTT.

Keywords Ovarian tissue transplantation · BNIP3 · Autophagy · mTOR/ULK1 pathway

Introduction

Ovarian tissue transplantation (OTT) is an effective and promising way of preserving fertility in patients with tumor disease requiring gonadotoxic chemotherapy/radiotherapy or bone marrow transplantation, patients with benign disease at high risk of ovarian failure, or women who have to delay childbearing for personal reasons [1]. OTT is also the only option of fertility preservation for young female and prepubertal children who require immediate cancer treatment, according to the updated guidelines of the American Society for Clinical Oncology (ASCO)[2]. A multicenter and large-sample study in 2021 revealed that the ovarian endocrine function resumption, pregnancy, and live birth rates after undergoing OTT were 95%, 38%, and 26%, respectively [3]. According to related studies, more than 200 newborn infants benefited from OTT [4]. OTT has been applied as a routine therapeutic approach for fertility preservation in many countries. However, the technique has certain limitations. The most prominent limitation of OTT is the extensive primordial follicle loss shortly after the transplantation procedure, referred to as the burnout effect. Gavish et al. observed approximately 83–92% of primordial follicle loss in ovarian grafts from all species 3 days post-transplantation and no further extensive depletion 7 days post-transplantation by subcutaneously transplanting marmoset, bovine, human ovarian cortical tissue into immunodeficient castrated

✉ Mujun Li
lmj1360@163.com

Fengxia Liu
liufengxia34@163.com

[1] Guangxi Medical University, Nanning 530021, China

[2] Department of the Reproductive Medicine Research Center, The First Affiliated Hospital of Guangxi Medical University, Nanning 530021, China

male mice [5]. Another study dynamically monitored the oxygen pressure of ovarian grafts, and the results revealed that the ovarian tissue was in a significant hypoxia state 5 days post-transplantation [6]. Because the sharp reduction in primordial follicles occurred exactly in the hypoxia period after grafting, hypoxia injury was considered to be a core contributor to primordial follicle loss. The primordial follicle is the only unit of the ovarian reserve in the mammalian ovary; it cannot be re-generated and progressively decreases with age. Ovarian function failure occurs when the primordial follicles are depleted. Therefore, the remaining number of primordial follicles determines ovarian lifespan after transplantation. Elucidation of the molecular mechanism of primordial follicle loss is of great clinical significance, which is beneficial for the development of protective pharmaceuticals for OTT and improvement of clinical outcome. However, the precise underlying mechanisms are largely unknown. Certain studies suggest that the hypoxia death of the primordial follicle is related to cell apoptosis and cell pyroptosis [7–9]. The hypotheses remain controversial because the administration of apoptosis or pyroptosis inhibitors (like sphingosine-1-phosphate, Z-VAD-FMK, Ac-YVAD-CMK) has unsatisfactory results and can only partially reduce follicle loss [7, 10]. Furthermore, it is unclear whether other signal pathways are involved in follicle loss after OTT. Autophagic pathway overlaps with apoptosis by sharing upstream molecules, and complex crosstalk occurs between autophagy and apoptosis [11]. It has been hypothesized that the autophagy may be involved in the massive follicle loss caused by hypoxic damage [12].

Autophagy, a type of programmed cell death, is a biological process of cytoplasmic cargo degradation through lysosome [13]. Numerous cellular functions including adaptation to stress, and maintenance of cellular homeostasis, development, and differentiation, indicate autophagy. The classical autophagic process has four steps: the formation and expansion of autophagosomes, fusion of autophagosomes with lysosomes, and degradation of autophagosome–lysosome contents. This dynamic process is finely regulated by autophagy-related genes (ATG). Autophagy is primarily inhibited by the mammalian target of rapamycin/Unc-51-like kinase 1 (mTOR/ULK1) pathway. When mTOR is inactivated, the downstream molecule ULK1 is phosphorylated to induce autophagy. The mTOR/ULK1 pathway plays a key role in the initiation of autophagy [14]. Autophagy serves as a double-edged sword in disease development. On one hand, autophagy at the basal level promotes cell survival in physiological conditions; on the other hand, inappropriate autophagy promotes cell death under stress conditions such as nutrition deprivation and hypoxic injury. Autophagy is expressed in both granulosa cells (GCs) and oocytes of the ovary; however, it seems to play various cell fate roles in different types of cells [15]. Oocytes are surrounded by GCs. There is cell-talk between the two types of ovarian cells by being closely regulated by gap junction formation [16]. GCs are more active than oocytes and exhibit a more rapid reaction to change in the ovarian microenvironment, which can influence the process of oocyte development and atresia by exchanging energy and metabolic products with oocytes. As mentioned before, follicle loss, especially the excessive depletion of primordial follicles, has a major impact on the outcome of OTT. Primordial follicle is composed of an oocyte enveloped by single-layer flattened GCs. The autophagy activity in GCs of primordial follicles seems to be an avenue for exploration of the mechanism of primordial follicle loss after OTT. A recent study reported increasing autophagy activity in GCs detected by transmission electron microscopy and immunofluorescence at 2 days after OTT [17]. No further details on the relationship between autophagy and OTT have been reported yet.

In the present study, the differentially expressed genes (DEGs) in human ovarian tissue after xenografting and non-grafted ovarian tissue were analyzed through bioinformatics protocol. We then located the autophagy/hypoxia-related gene Bcl-2/adenovirus E1B 19-kDa interacting protein 3 (BNIP3), which is identified as the hub gene during OTT, using the MCODE plugin from Cytoscape. The expression of BNIP3 and autophagy activity was examined in tissues and cells by immunohistochemistry staining, transmission electron microscopy (TEM), qPCR, western blotting, and fluorescence staining. We explored the impact of BNIP3-induced autophagy in GCs of primordial follicles using a mice ovarian auto-transplantation model and hypoxia-mimicking KGN cells, which provided novel evidence of a possible connection between BNIP3-media autophagy and primordial follicle loss after OTT.

Materials and methods

Bioinformatic protocols and hub gene identification

The GSE47555 dataset was downloaded from the Gene Expression Omnibus (GEO) database (www.ncbi.nlm.nih.gov/geo). GSE47555 is an expression profile dataset based on GPL571 (Affymetrix Human Genome U133A 2.0 Array). The experimental tissues of the GSE47555 dataset included human ovarian fragment xenografted in nude mice for 7 days ($n=4$) and non-grafted human ovarian fragment ($n=4$) after freezing–thawing. DEG analysis was conducted using an interactive web tool, GEOR2. Boxplots generated using the GEO2R tool were used to display gene expression values and determine whether the samples were suitable for differential expression analysis. DEGs were visualized using a volcano plot. Genes were considered significantly differentially expressed with absolute log fold change (llog

(FC)|) > 1 and $P < 0.05$. Metascape software (http://metascape.org/gp/index.html) was used for Kyoto Encyclopedia of Genes and Genomes (KEGG) pathway enrichment analysis. P value < 0.05 was considered statistically significant. The protein-to-protein interaction (PPI) network was constructed using the STRING database (https://www.string-db.org/) (v11.0). The significant modules of the PPI network were inferred using the Molecular Complex Detection (MCODE) plugin of Cytoscape (version 3.8.2). The filtering parameters were set as follows: MCODE sores were set to > 5, degree cutoff to 2, node score cutoff to 0.2, K-core equal to 2, and max depth to 100. The top 100 genes were downloaded from GeneCards database (http://www.genecards.org/) based on the search terms "hypoxia" and "autophagy." The intersection of hub genes and hypoxia-autophagy related genes was determined using a Venn diagram online tool (http://bioinformatics.psb.ugent.be/webtools/Venn/).

Experimental animals and ovarian auto-transplantation procedure

Fifteen 6- to 8-week-old female C57BL/6 mice provided by Guangxi Medical University Laboratory animal center were used in the present study. All mice were housed in a Special Pathogen Free (SPF) environment. They were randomly divided into three groups comprising 5 mice each: control group, auto-transplanted group, and 3-methyladenine (3-MA) group. The control group was not subjected to any procedure; the transplanted groups had ovaries transplanted in their back muscle under anesthesia and by intraperitoneal injection with 0.2 ml/10 g 1.25% Avertin (M2910, Easycheck, Nanjing, China). 3-MA, as a specific inhibitor of autophagy, has been reported to block autophagy at a dose of 10 mg/kg following intraperitoneal administration in myocardial injury mice models [18]. In the present study, the mice in the 3-MA group were intraperitoneally injected with 10 mg/kg/day 3-MA (HY-19312, MCE, USA). The auto-transplantation procedure was completed in 30 min. The ovarian surgical day was designated as day 0. The fresh ovaries from the control group and the ovary grafts from the auto-transplanted group and 3-MA group were collected at day 2, day 3, day 7, and day 14 for different analyses.

Histological evaluation and follicle estimation

The ovaries were fixed and embedded in paraffin wax which was sequentially sectioned at 5-μm thickness. Every fifth section of each sample was stained with hematoxylin-and-eosin (H&E) for later follicle counting under a light microscope [19]. The total number of follicles in all the slices of each ovary from different groups (five ovaries per group) was evaluated. Follicles were categorized into primordial, primary, secondary, and antral follicles based on the morphological appearance of the granulosa cell [20]. Primordial follicles were defined as the oocyte surrounding a single layer of flattened pre-granulosa cells. Primary follicles were characterized as the oocyte surrounding a single layer of cuboidal granulosa cells. Secondary follicles have multiple layers of cuboidal granulosa cells without antral space. Antral follicles had multiple layers of granulosa cells with antral space. Secondary and antral follicles were regarded as only those with a visible oocyte nucleus avoided for double-counting.

Transmission electron microscopy analysis

The ovarian fragments were fixed and prepared into ultrathin sections. The sections were subsequently examined using TEM (HITACHI, HT7700, Japan). The ultrastructural evaluation was performed in the subcapsular region of the ovarian cortex to evaluate the primordial follicle structures. A quantitative analysis of the autophagic vacuoles in at least 3 randomly selected GCs of primordial follicle from different groups was conducted.

Immunohistochemistry staining

The paraffin sections were incubated with anti-SQSTM1/p62 rabbit pAb (GB11531, Servicebio, Wuhan, China) at 1:1000 dilution, anti-LC3A/B rabbit pAb (GB11124, Servicebio, Wuhan, China) at 1:200 dilution, anti-Beclin 1 rabbit pAb (GB11228, Servicebio, Wuhan, China) at 1:1000 dilution, and anti-BNIP3 rabbit pAb (GB11204, Servicebio, Wuhan, China) at 1:1000 dilution overnight at 4 °C. After rinsing, HRP conjugated goat anti-rabbit IgG (H + L) (GB23303, Servicebio, Wuhan, China) at 1:200 dilution was added for 60 min at room temperature (about 25 °C). The sections were observed under a light microscope (Olympus, Tokyo, Japan). Three sections were obtained from each ovary in the control, OTT-3D (at 3-day post-transplantation), and OTT-3D + 3-MA (at 3-day post-transplantation with 3-MA) groups, and the proteins (BNIP3, Beclin-1, LC3B, and SQSTM1/p62) in all the GCs of primordial follicle in each section were analyzed based on the average optical density (AOD), using ImageJ (https://imagej.nih.gov/ij/download.html). The IHC-positive tissue (Mice kidney) was assigned as positive control, and replacement of primary antibody with PBS was used as a negative control.

Cell line and culture

The human ovarian granular tumor cell line (KGN) was obtained from FENG HUI SHENG WU (Hunan, China). The KGN cell line was authenticated using short tandem repeat (STR) analysis performed by TSINGKE Biological Technology (Hunan, China). The cells were cultured with

Dulbecco's modified Eagle's medium (DMEM, Gibco; California; USA) with 10% fetal bovine serum (FBS; Gibco; California; USA) and 1% penicillin/streptomycin (Gibco; California; USA) with 5% CO_2 in a 37 °C incubator. For autophagy-related experiments, cells were treated with 100 nM bafilomycin A1 (HY-100558, MCE, USA) or 10 μM MHY1485 (HY-B0795, MCE, USA) for 4 h according to the product instructions.

Cytotoxicity analysis

A CCK8 Kit purchased from APExBIO (Houston, TX, USA) was used for the CCK8 assay cytotoxicity analysis of $CoCl_2$. KGN cultured in a 96-well plate (1 × 10^4 cells/well) was treated with $CoCl_2$ (C8661, Sigma-Aldrich, St Louise, MO, USA) at different concentrations (50 μM, 100 μM, 200 μM, 400 μM, and 800 μM). The cell wells without $CoCl_2$ were set as a blank group, and the cell-free wells with DMEM only were set as the negative group. There were at least three replicate wells for each group. After 72 h of treatment, each well was replaced with 100 μl DMEM and 10 μl CCK-8 solution and incubated at 37 °C for 1 h. The absorbance at 450 nm was measured using the Varioskan™ LUX multimode microplate reader (ThermoFisher Scientific, Vantaa, Finland).

Hypoxia-mimicking cell model

The KGN cell treated with $CoCl_2$ was selected to mimic hypoxia conditions according to a previous study [21]. The exact concentration of $CoCl_2$ was based on the cytotoxicity analysis. The cells were incubated with 200 μM $CoCl_2$ for 24 h. The cells with a complete medium without $CoCl_2$ were set as the control. The stable expression of Hypoxia Inducible Factor 1 Subunit Alpha (HIF1A) protein served as an important evaluation metric of the hypoxia model.

Cell transfection

BNIP3-overexpression (and the corresponding negative control lentivirus) and siRNA-BNIP3 (and the corresponding negative control lentivirus) lentiviruses were purchased from Jikai Gene (Shanghai, China). The BNIP3-overexpression vector was GV492 (Ubi-MCS-3FLAG-CBh-gcGFP-IRES-puromycin). The siRNA-BNIP3 vector was GV493 (hU6-MCS-CBh-gcGFP-IRES-puromycin). Cells were transfected with BNIP3-overexpressing lentivirus, siRNA-BNIP3 lentivirus, and the corresponding negative control lentivirus (NC). Stable cells were generated after 2 μg/ml puromycin (ST551, Beyotime, Shanghai, China) selection. The sequence of siRNA-BNIP3 is gaACTGCACTTCAGCAA TAAT and that of the corresponding negative control siRNA TTCTCCGAACGTGTCACGT.

Quantitative real-time polymerase chain reaction

The total RNA of KGN cells from the control and $CoCl_2$ groups was extracted using the RNAsimple Total RNA Kit (TIANGEN BIOTECH, Beijing, China). RNA samples were further reverse-transcribed into cDNA with TaKaRa PrimeScriptTM RT Master Mix (Perfect Real Time) (Cat. #RR036A). The qRT-PCR was performed using TaKaRa TB Green® Premix Ex TaqTM II (Tli RNaseH Plus) (Cat. #RR820A) on an Applied Biosystems 7500 Real-Time PCR instrument (Thermo Fisher SCIENTIFIC, USA). The primer sequences employed are listed in Table 1. The relative amplification of the mRNAs was determined based on the quantitation-comparative CT (△△CT) method, with Actin Beta (ACTB) as the RNA endogenous control.

Western blotting analysis

Total proteins were extracted using a precooled RIPA lysis buffer (P0013B, Beyotime, Shanghai, China) with 100 mM PMSF (ST505, Beyotime, Shanghai, China) on ice. The protein concentrations were determined using an Enhanced BCA Protein Assay Kit (P0010, Beyotime, Shanghai, China). A total of 20 μg protein was loaded into each lane, separated by SDS-PAGE (8% and 12%), and then transferred to 0.2/0.45 μm PVDF membranes (Merck Millipore, Bedford, USA). Furthermore, 5% fat-free milk was used to block the PVDF membranes for 1–2 h at room temperature (about 25 °C). The membranes were incubated with primary antibodies at 4 °C overnight. The antibodies used were as follows: anti-BNIP3 (ab109362, Abcam, Canada) at 1:1000 dilution, anti-HIF-1 alpha (ab179483, Abcam, Canada) at 1:1000 dilution, anti-Beclin-1 (11306–1-AP, Proteintech, Wuhan, China) at 1:8000 dilution, anti-LC3B (14600–1-AP, Proteintech, Wuhan, China) at 1:2000 dilution, and anti-P62/SQSTM1 (18420–1-AP, Proteintech, Wuhan, China) at 1:5000 dilution. Anti-Beta actin (20536–1-AP, Proteintech, Wuhan, China) at 1:4000 dilution was set as an internal reference. The membranes were incubated with goat anti-rabbit IgG (H + L) secondary antibody, HRP (31,460, Invitrogen) for 1 h at room temperature (about 25 °C). The ImageJ was applied to the quantitative evolution of protein bands from different samples. Each sample was tested independently in

Table 1 Primer sequences applied for quantitative real-time polymerase chain reaction

Genes	Primer sequences (5′-3′)
BNIP3	Forward: GCAATAATGGGAACGGGGGC
BNIP3	Reverse: ACTCCGTCCAGACTCATGCT
Actin beta	Forward: CCTTCCTGGGCATGGAGTC
Actin beta	Reverse: TGATCTTCATTGTGCTGGGTG

triplicate. The relative expression levels were determined using the ratio of the total protein to the β-actin protein, whereas those of phosphorylated proteins were determined relative to that of total protein.

Autophagy detection by DALGreen

KGN cells were incubated with 1000 µl of a 0.6 µM DALGreen working solution (D675, Dojindo Laboratories, Shanghai, China) at 37 °C for 30 min. After removing the culture medium and washing with PBS twice, the KGN cells were treated with 200 µM $CoCl_2$. After treatment for 24 h, KGN cells were observed under confocal laser-scanning microscopy (Leica TCS SP8 STED, Leica, Germany). Cells were considered autophagy-positive when they displayed more than three DALGreen puncta [22]. The intensity of the green fluorescence is proportional to the autophagy activity.

Autophagy flux detection by LC3B with immunofluorescence staining

KGN cells were incubated with 1:1000 diluted anti-LC3B (14600–1-AP, Proteintech, Wuhan, China) at 4 °C overnight after being fixed and blocked. Then, KGN cells were incubated with 1:1000 diluted anti-Rabbit IgG from immunofluorescence staining kit (P0179, Beyotime, Shanghai, China) at room temperature (about 25 °C) for 1 h (protected from light). Nuclei were counterstained with DAPI (C0065, Solarbio, Beijing, China) for 5 min. Following the addition of the anti-fluorescence quencher, the samples were observed and the images were analyzed under a fluorescence microscope (IX71 + DP73 + cellSens Dimension, Olympus, Tokyo, Japan). LC3B immunofluorescence staining was quantified by estimating the percentage of LC3B puncta over total cell number in three different fields [23]. LC3B puncta and cell number quantification was performed using ImageJ software.

Statistical analyses

The results in this study are displayed as mean ± SD, based on at least three independent experiments. Data from two groups were compared using *t*-tests (equal variances data) or nonparametric tests (unequal variances data). All the statistical analyses were performed using GraphPad Prism 9 for macOS (version 9.3.1) (GraphPad Software, San Diego, CA, USA). Statistical significance was set at $P < 0.05$.

Results

BNIP3 was identified as a hub gene during ovarian tissue transplantation

To determine significant genes involved in the ovarian transplantation procedure, an expression profile microarray of non-grafted ovarian and grafted ovarian from the GEO database was analyzed. The distributions of samples were viewed using the GEO2R tool, and the median-center value indicated that the data were normalized and cross comparable (Fig. 1a). The volcano plots are shown in Fig. 1b. There were 2613 DEGs detected from GSE47555, 803 of which were upregulated and 1810 downregulated. The DEGs were uploaded onto Metascape to allow for KEGG enrichment analysis. As shown in Fig. 1c, the results reveal that the "autophagy-animal" pathway was enriched in downregulated DEGs. To explore the functional relationships among DEGs and identify the essential proteins, a PPI network was established using STRING, and key protein clusters were screened by MCODE in Cytoscape. Eight modules, including 424 hub genes, were identified. The hub gene is a gene that is highly interconnected in the network, with major biological significance. Considering the aim of the present study was to reveal specific genes related to autophagy in hypoxia condition, we obtained five genes related to both hypoxia and autophagy from the GeneCards database and intersected them with hub genes. The results showed that only BNIP3 was identified (the Venn diagram in Fig. 1d). Based on the results, we hypothesized that BNIP3-induced autophagy is essential during OTT procedure; therefore, we selected BNIP3 for subsequent experiments.

Morphological characteristics and follicle count in back muscle auto-transplanted ovaries of mice

To verify the hypothesis, autografted models were established by transplanting the ovary into the back muscle of the same mice. To ensure all the ovaries were at the same development condition, the mice from different groups were the same age and of similar weight (15–18 g) when their ovaries were collected. Histological examination showed a remarkable reduction in the number of follicles at different stages in the transplanted ovaries when compared with the fresh ones, which is consistent with the findings of previous studies. Only certain primordial follicles were found in the margins of ovarian cortex 3 days post-transplantation; all the antral follicles and a large part of secondary follicles were atretic with disorganization of ovarian medulla tissue (Fig. 2a–c). Normal follicles at

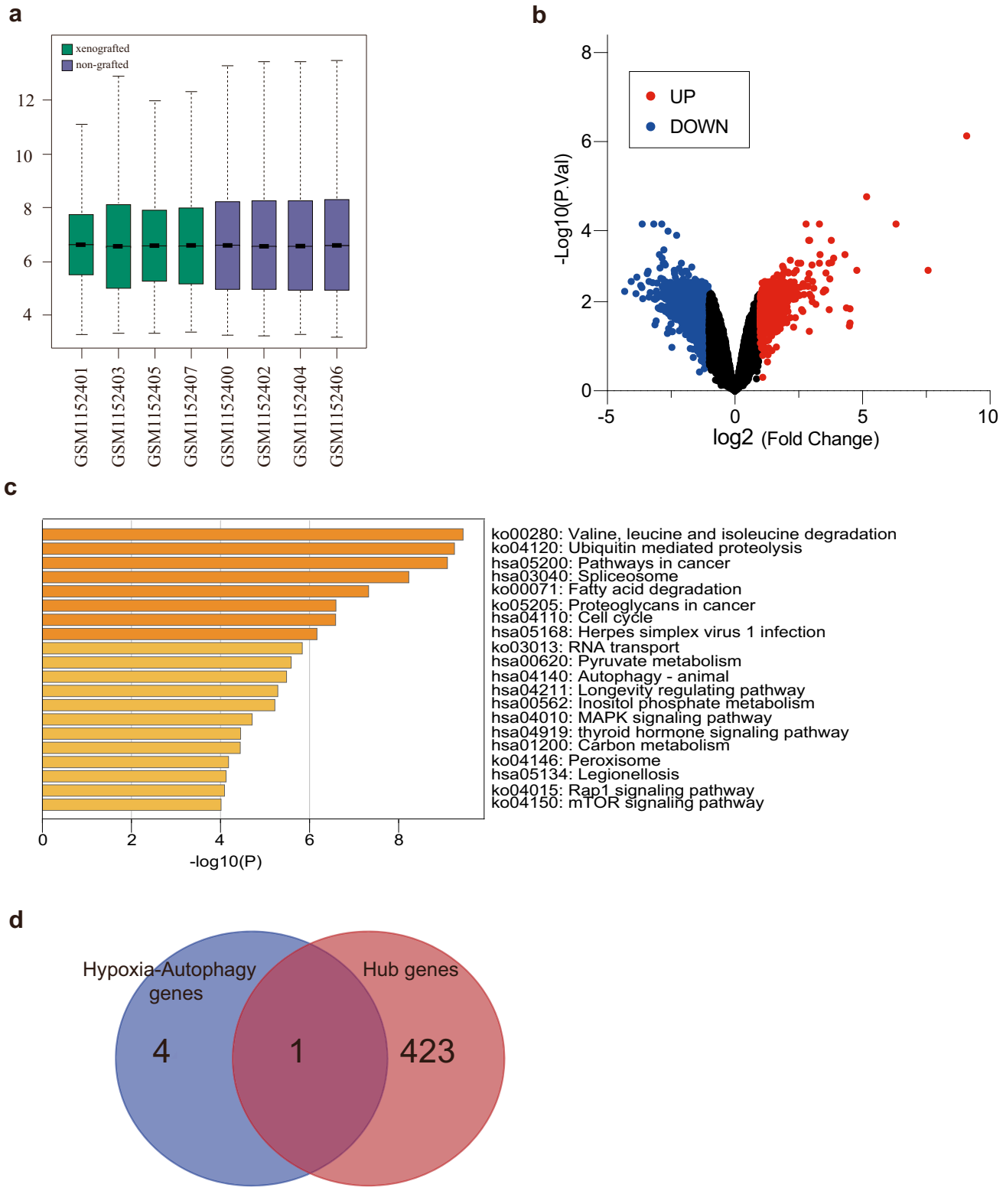

Fig. 1 Identification of hub genes in human ovarian tissue xenografting procedure. **a** Boxplot of distribution for sample values. **b** Volcano plot of differentially expressed genes (DEGs) in GSE47555. The reds indicate the upregulated genes and the blues downregulated genes. **c** Kyoto Encyclopedia of Genes and Genomes (KEGG) enrichment analysis. Top 20 KEGG enriched pathways sorted by − log10(P) in the downregulated DEGs analyzed by Metascape. **d** Venn-diagram of hypoxia-autophagy genes and hub genes. The overlapping section represents the hypoxia-autophagy genes screened from GeneCards and hub genes selected by MCODE plugin from Cytoscape

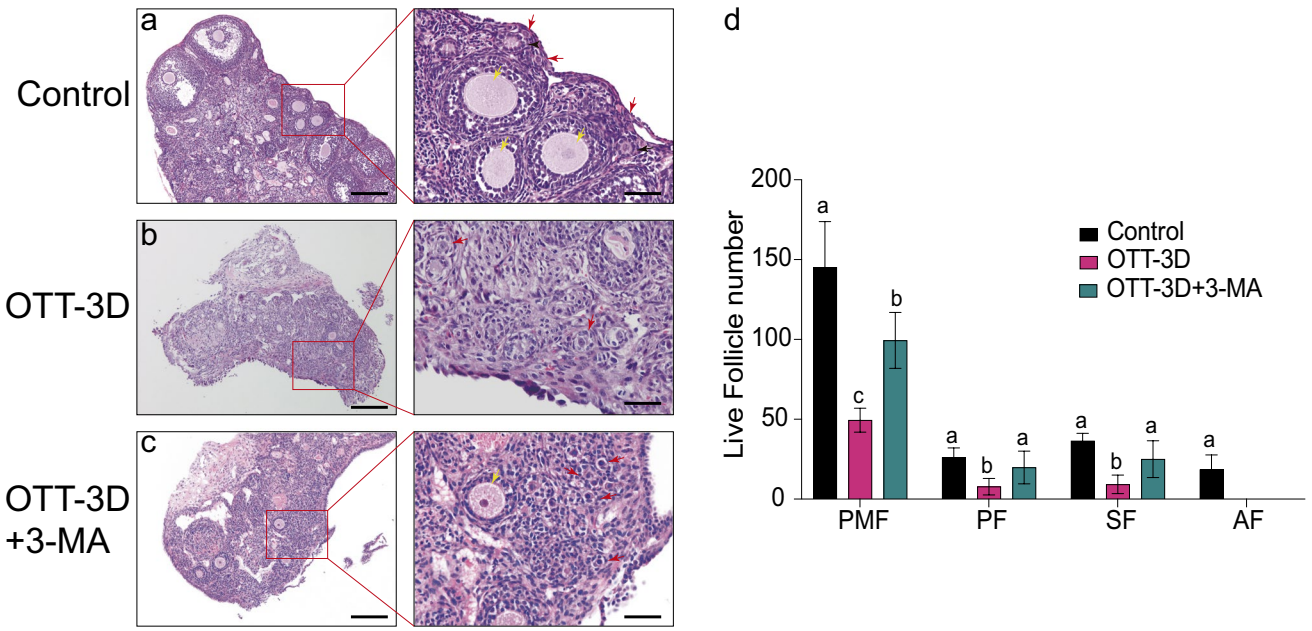

Fig. 2 Morphological characteristics and follicle count. **a** Histological observation of the ovaries of mice from the control group. **b** Histological observation of the ovaries of mice from the auto-transplantation group at day 3 after transplantation (OTT–3D). **c** Histological observation of the ovaries of mice from the 3-MA group at day 3 after transplantation (OTT–3D + 3-MA). Figures on the right represent zoomed-in views of the area outlined in red dashed lines in the left figures. Scale bars represent 200 μm and 50 μm for left and right figures, respectively. Red arrows represent primordial follicles; black arrows represent primary follicles; yellow arrows represent secondary follicles. **d** Follicle quantity at different stages from the control group, OTT–3D group, and OTT–3D + 3-MA group. Character (a, b, c) differences of same stage follicles were significant ($P < 0.05$). PMF primordial follicle, PF primary follicle, SF secondary follicle, AF antral follicle

different stages occurred again 7 and 14 days after transplantation with or without 3-MA, and the ovarian tissue began to attach to the back muscle closely (Fig. S1), which demonstrated that ovaries survived at the grafted site eventually. Subsequently, we applied an autophagy inhibitor, 3-MA, to investigate the role of autophagy in primordial follicle loss after grafting. The ovaries administered with 3-MA 3 days post-transplantation showed more primordial follicles and less injury of medulla than the untreated group (Fig. 2b–c). The follicles of different stages from the control group, OTT–3D group, and OTT–3D + 3-MA group were counted separately according to follicle categorization, as mentioned in the "Materials and methods," by counting all the serial sections of five similar-sized ovaries from each group. An average of 50 serial Sects. (5 μm per section, spaced 25 μm) was obtained from each ovary. The follicle counts are presented in Fig. 2d and Table 2. Different characters (a, b, c) of the same stage follicle indicated significant difference ($P < 0.05$). The primordial, primary, secondary, and antral follicles were significantly decreased in the OTT–3D group, when compared with in the control group ($P < 0.05$), whereas the number of primordial follicles was significantly higher in the OTT–3D + 3-MA group than in the OTT–3D group ($P < 0.05$).

Ultrastructure features detected using transmission electron microscopy

To clarify the autophagy activity of GCs post-transplantation, ultrastructural investigations were carried out

Table 2 Follicle quantification at different stages from different groups

Groups	PMF (mean ± SD)	PF (mean ± SD)	SF (mean ± SD)
Control Group	145 ± 29a	26 ± 6a	36 ± 5a
Auto-transplantation Group	49 ± 8c	8 ± 5b	9 ± 6b
3-MA Group	99 ± 18b	20 ± 10a	25 ± 12a

Data from the same columns were analyzed statistically using the *t*-test. Different characters (a, b, c) within the same column indicated a significant difference ($P < 0.05$)

PMF primordial follicle, *PF* primary follicle, *SF* secondary follicle, *3-MA* 3-methyladenine, *SD* standard deviation

using TEM to visualize autophagic vacuoles. The typical autophagic vacuole with parallel membrane formed in the autophagy process, including autophagosomes and autophagosome–lysosome, is distinctly visible through TEM. As shown in Fig. 3, only a degradation autophagic vacuole was observed occasionally in the cytoplasm of GCs from the fresh ovary. The GCs of the ovary on day 2 after grafting displayed a complete cell structure with normal organelle distribution, and several typical autophagosomes with double membranes were observed. The GCs of the ovary on day 3 after grafting showed more typical autophagosomes in cytoplasm with cytoplasmic contraction and heterochromatin in the nucleus. A quantitative analysis of the autophagic vacuoles in GCs of primordial follicle before and after transplantation was conducted (Fig. 3d). According to the results, the number of autophagic vacuoles in the cytoplasm of primordial follicle GCs increased after transplantation ($P < 0.05$, $P < 0.01$).

BNIP3 and autophagy were upregulated in mice ovaries after auto-transplantation

Immunohistochemistry was performed to indicate BNIP3 protein expression among different groups. The ovarian tissue was immuno-stained for target protein (brown area) and hematoxylin-stained for nuclei (blue area). IHC, a method of semiquantitative and localization analysis, has an advantage of showing the expression level and location of target protein. As shown in Fig. 4a–c, BNIP3 expression was distributed in GCs, oocytes, and stroma cells of the ovary from different groups. In the transplantation groups with or without 3-MA treatment, deeper staining of BNIP3 was noted in GCs of primordial follicles when compared with the fresh ovarian tissue from the control group. The expression of BNIP3 in GCs of primordial follicles was similar both in OTT-3D and OTT-3D + 3-MA group. Positive control for BNIP3 demonstrates positive staining, and the absence of BNIP3 staining in negative control indicated the specificity of the BNIP3 antibody (Fig. 4d, e). Expression of BNIP3 among groups was quantitatively analyzed by AOD. There was a significant increase of BNIP3 between control and transplantation group ($P < 0.05$) while no significant difference between OTT-3D and OTT-3D + 3-MA group (Fig. 4r). The results indicated that BNIP3 expression in GCs of primordial follicle was upregulated after transplantation, and the 3-MA treatment had no effect on BNIP3 expression.

The autophagy activity was also evaluated among different groups using immunohistochemical staining for autophagy-related protein (Beclin-1, LC3B, SQSTM1/p62) expression in the GCs of primordial follicles. Beclin-1 is

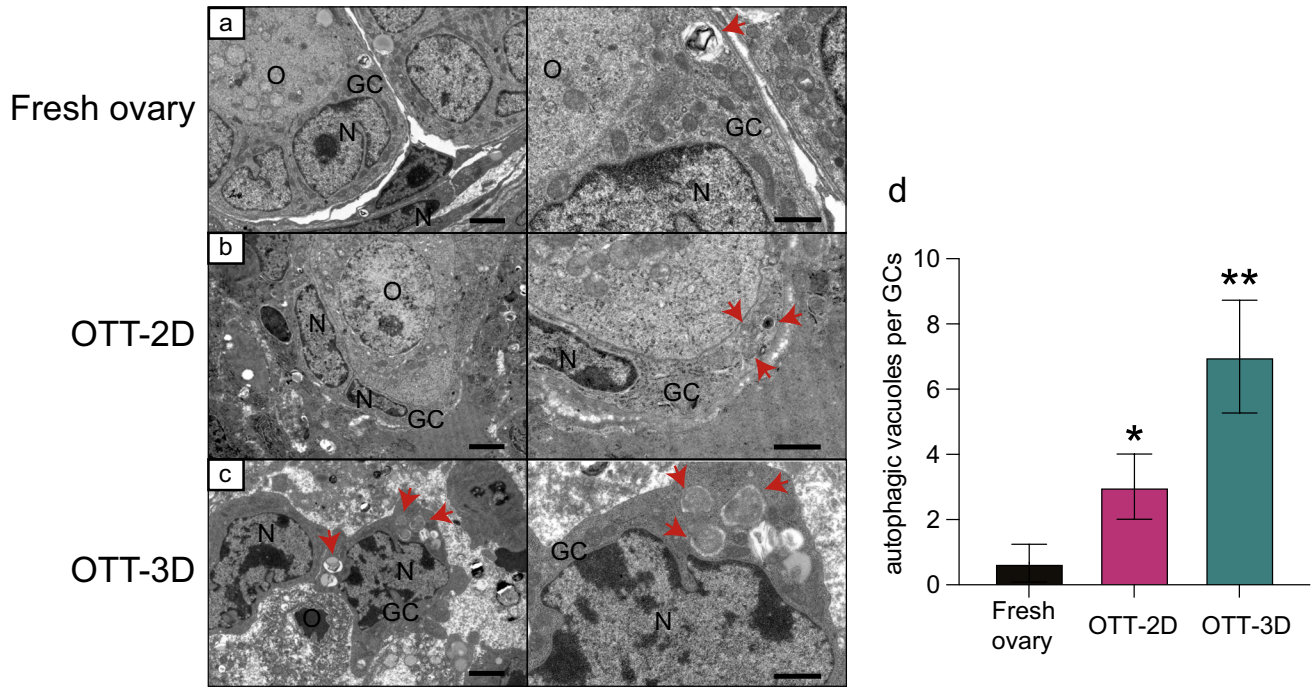

Fig. 3 Ultrastructure of autophagy was examined by TEM in mice GCs **a** fresh ovary. **b** auto-transplanted ovary on day 2 (OTT–2D). **c** Auto-transplanted ovary on day 3 (OTT–3D). The right figure is an enlargement of the left figure. Scale bars represent 2 μm and 1 μm for the left and right figures, respectively. Red arrows represent the autophagic vacuole. **d** Quantitative analysis of the autophagic vacuoles in GCs of primordial follicles. Columns and bars represent the mean ± SD. *$P < 0.05$; **$P < 0.01$. O oocytes, GCs granulosa cells, N nucleus

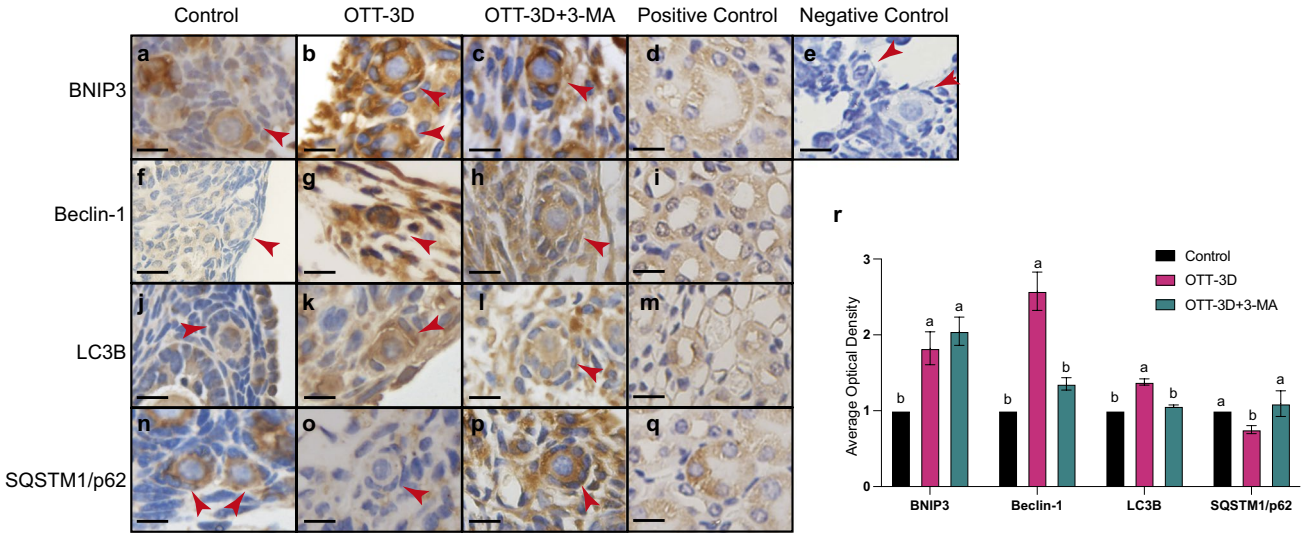

Fig. 4 Immunohistochemical analysis of BNIP3 and autophagy-associated protein in the ovaries of mice. **a**, **b**, **c**, **d** BNIP3 protein expression of the control group, OTT-3D, OTT-3D + 3-MA group and positive control. **e** Negative control with PBS. **f**, **g**, **h**, **i** Beclin-1, protein expression of the control group, OTT-3D, OTT-3D + 3-MA group, and positive control. **j**, **k**, **l**, **m** LC3B protein expression of the control group, OTT-3D, OTT-3D + 3-MA group, and positive control. **n**, **o**, **p**, **q** SQSTM1/p62 protein expression of the control group, OTT-3D, OTT-3D + 3-MA group, and positive control. Red arrows represent primordial follicles. Scale bar represents 10 μm. **r** Quantification of protein expression level. Different letters (a, b, c) in the same-stage follicles indicate significant differences ($P < 0.05$). OTT-3D ovarian tissue transplantation at day 3, OTT-3D + 3-MA; ovarian tissue transplantation with 3-MA treatment at day 3

essential to initiating and positively regulating autophagy. LC3B is a well-established positive molecular marker of autophagy. SQSTM1/p62 can directly bind to LC3B and is the most extensively studied among the substrates degraded by autophagy. Therefore, it is inversely correlated with autophagic activity [24]. The immunohistochemistry staining results indicated that Beclin-1, LC3B expression increased while SQSTM1/p62 expression decreased in the transplantation group compared with the control group. Beclin-1, LC3B expression decreased while SQSTM1/p62 expression increased in OTT-3D + 3-MA group compared with the OTT-3D group. Positive control for Beclin-1, LC3B, and SQSTM1/p62 demonstrates positive staining. The results are shown in Fig. 4f–q. There was a significant difference of those proteins in OTT-3D group and control, OTT-3D + 3-MA group ($P < 0.05$) according to the quantification results (Fig. 4r). The results suggested that autophagy was upregulated after transplantation and downregulated to the basal level upon 3-MA administration.

BNIP3 and autophagy were upregulated in hypoxia-mimicking model induced by $CoCl_2$

Since BNIP3 and autophagy activation in GCs of primordial follicles after OTT was observed in vivo experiments, we further investigated BNIP3 expression and autophagy activity in response to the hypoxia condition in vitro by utilizing KGN cell line. KGN cell maintains the similar physiological characteristics of ovarian granulosa cells, which is considered as a useful in vitro model of ovarian GCs to study the physiological and pathophysiological status of ovary [25–28]. A hypoxia cell model treated with $CoCl_2$ was established in KGN cell. $CoCl_2$-induced hypoxia, which increases HIF1A protein level in a dose and time-dependent manner, is one of the most commonly used methods in hypoxia experiments [21]. Determination of the optimal concentration of $CoCl_2$ was based on the cytotoxicity results obtained by the CCK8 assay. The cell viability in cells treated with 50 μM, 100 μM, and 200 μM $CoCl_2$ was more than 80% when compared with that of the control group, while 400 μM and 800 μM $CoCl_2$ treatment decreased the percentage of living cells by more than 20% (Fig. 5a). In addition, western blotting analysis showed that the HIF1A expression level was increased in 200 μM $CoCl_2$ treatment for 24 h (Fig. 5b). Based on the results, a concentration of 200 μM $CoCl_2$ for 24 h treatment was selected to establish the hypoxia-mimicking cell model in the subsequent experiments. Subsequently, BNIP3 gene and protein expression in the hypoxia condition were assessed by qPCR and western blotting, respectively. BNIP3 mRNA expression was significantly increased following $CoCl_2$ incubation for 24 h compared with the control ($P < 0.05$), which is consistent with the alteration in protein level expression (Fig. 5c–d). Subsequently, the role of autophagy under hypoxia in KGN cells was examined through different methods. The key autophagy proteins, including Beclin-1, LC3B, and SQSTM1/p62, were detected

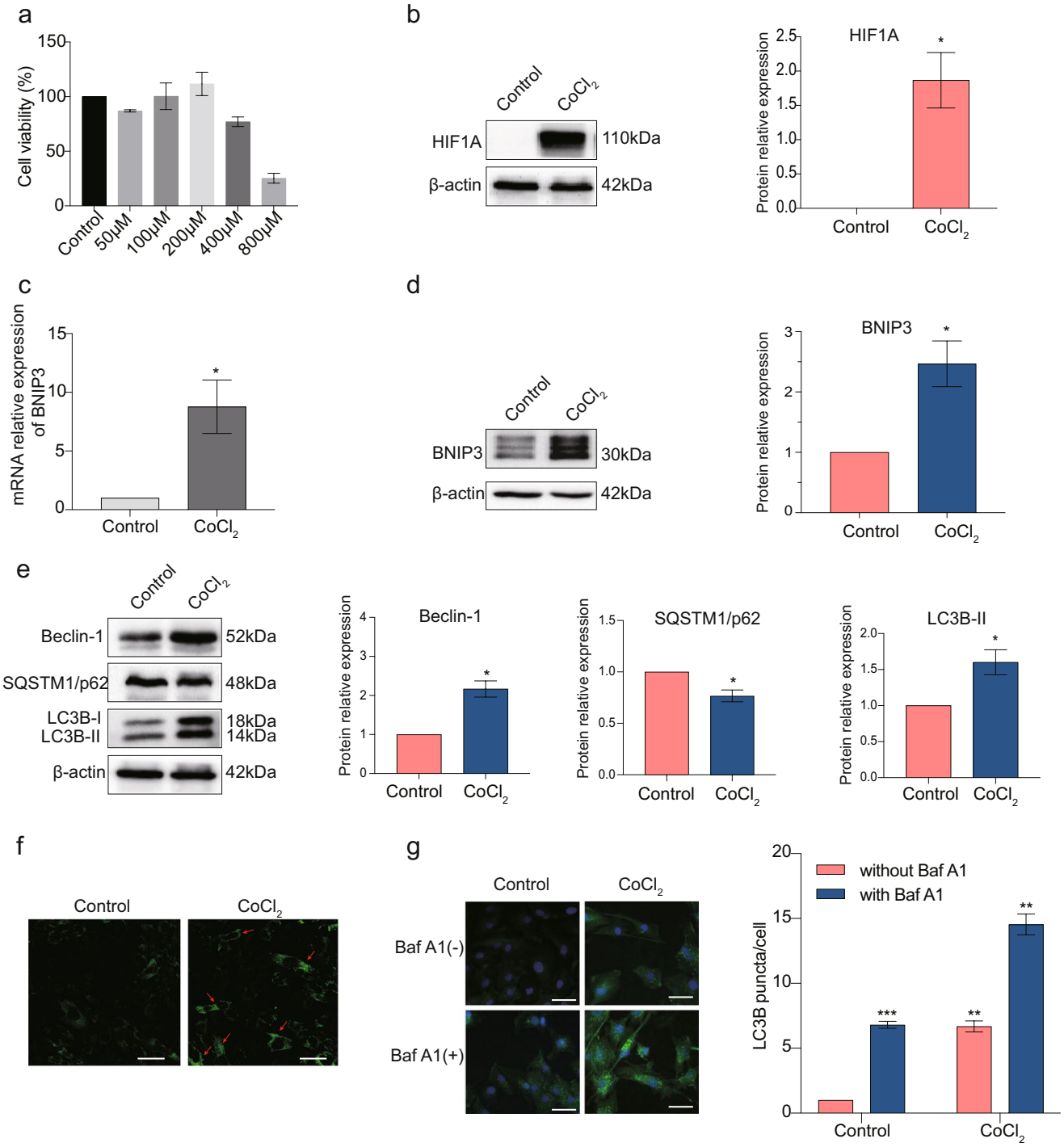

Fig. 5 BNIP3 and autophagy was upregulated in the hypoxia-mimicking model induced by $CoCl_2$. **a** The cytotoxicity of different concentration $CoCl_2$ (50 μM, 100 μM, 200 μM, 400 μM, 800 μM) by CCK8 assay. **b** HIF1A protein expression in KGN cells treated with 200 μm $CoCl_2$ at 24 h compared with control group. **c** BNIP3-mRNA expression with 200 μM $CoCl_2$ incubation was determined by qRT-PCR within 24 h (β-actin was used as a reference gene). **d** BNIP3 protein expression with 200 μM $CoCl_2$ incubation was determined by western blotting analysis. **e** Autophagy-related protein expression with 200 μM $CoCl_2$ incubation was determined by western blot analysis. **f** Autophagy activity in KGN cells was detected by DALGreen staining. The green fluorescence puncta represent the autophagic vacuoles, and the red one autophagic-positive cells. Scale bar represents 50 μm. **g** Immunofluorescence analysis and quantification of LC3B protein in $CoCl_2$-incubated KGN cells in the presence or in the absence of Baf A1. The green fluorescence puncta were regarded as autophagosome-band LC3B-II. The number of LC3B-II puncta positively correlates with the number of autophagosomes. The nucleus was detected through DAPI staining (blue). Scale bar represents 100 μm. Columns and bars represent the mean ± SD. $^{*}P < 0.05$; $^{**}P < 0.01$; $^{***}P < 0.001$. Baf A1; Bafilomycin A1

to assess autophagy activity by western blot analysis. As mentioned earlier, LC3B is a molecular marker of autophagy that is present in LC3B-I (non-lipidated) and LC3B-II (lipidated) form. The conversion of LC3B from cytosolic LC3B-I to lipidized LC3B-II (which localizes to the autophagosome membrane) indicates autophagosome formation. The western blotting analysis showed that the protein levels of Beclin-1 and LC3B-II increased in the hypoxia group when compared with that in the control group, while SQSTM1/p62 protein levels decreased (Fig. 5e). The results suggest that autophagy was activated by hypoxia induced by $CoCl_2$ in KGN cell.

A more direct method of autophagy identification is the evaluation of autophagic vacuoles, including autophagosomes and autophagosome–lysosome. DALGreen is a fluorescent dye that can be used for specific detection of autophagic vacuoles by inserting a double-membrane structure and emitting green fluorescence. The staining results showed that more DALGreen positive puncta were observed in the hypoxia group than in the control group, indicating autophagy upregulation by hypoxia (Fig. 5f).

Autophagy, including autophagic vacuole formation and degradation, is a dynamic process. Therefore, a combination of autophagic flux measurement and autophagic vacuole number detection is a more reliable method for assessing autophagy activity. The observation of LC3B turnover based on the degradation of LC3B-II in autophagosome–lysosome is a classical method of evaluating autophagic flux. As mentioned earlier, LC3B-I (appears diffusely in cytoplasm) is converted to LC3B-II (appears as puncta in the autophagosome membrane) to form the autophagosome. The autophagosome then fuses with a lysosome to generate an autophagosome–lysosome to complete autophagic degradation. If cells are treated with Bafilomycin A1 (an inhibition of autophagosome-lysosome fusion), the degradation of LC3B-II is blocked, and LC3B-II accumulates. Therefore, the LC3B-II, which is degraded, is measured (also known as autophagic flux) by determining the extent of its change with or without Bafilomycin A1 treatment[24]. As shown in Fig. 5g, LC3B-II puncta increased with Bafilomycin A1 treatment in the control group, while the difference in LC3B-II puncta in the presence and absence of Bafilomycin A1 was relatively pronounced under hypoxia conditions induced by $CoCl_2$. The results suggested that autophagic flux of KGN cell increased in response to hypoxia.

BNIP3 induced autophagy in hypoxia-mimicking model treated with $CoCl_2$

To elucidate the potential role of BNIP3 in the regulation of autophagy, the alteration of its activity after the overexpression and silencing of BNIP3 was investigated. First, mRNA and protein levels of BNIP3 were detected to confirm BNIP3 overexpression and low expression in KGN cell (Fig. 6a–d). Subsequently, the variation of autophagy-associated proteins including Beclin-1, LC3B, and SQSTM1/p62 affected by BNIP3 was explored through western blot analysis. Compared with the MOCK and negative control (NC) group, BNIP3 overexpressing cells displayed increased expression of Beclin-1, LC3B, and decrease of SQSTM1/p62; while BNIP3 silencing cells decreased expression of Beclin-1 and LC3B and increased SQSTM1/p62. The results suggest that BNIP3 induced autophagy in KGN cells (Fig. 6e–f). Further experiments were carried out to validate the relationship between BNIP3 and autophagy in hypoxic conditions. The results showed that BNIP3 silencing reversed the autophagy induced by $CoCl_2$ (Fig. 6g), indicating that BNIP3 could impact the autophagy process positively in KGN cell.

BNIP3 induced autophagy through the mTOR/ULK1 pathway under hypoxia

To determine if BNIP3 regulated autophagy through the mTOR/ULK1 pathway in hypoxia condition, we performed western blotting analysis and observed the protein expression levels of p-mTOR, p-ULK1, mTOR, and ULK1 in $CoCl_2$ treatment cells and BNIP3 overexpression/silencing cells. The protein level of phosphorylated-ULK1 (p-ULK1) was upregulated while phosphorylated mTOR (p-mTOR) was downregulated in KGN cells after $CoCl_2$ exposure, which indicated that hypoxia induced the mTOR/ULK1 pathway. Overexpression of BNIP3 could decrease p-mTOR expression and increase p-ULK1 expression. Moreover, the silencing of BNIP3 could increase p-mTOR and decrease p-ULK1. The effects of BNIP3-overexpression on the mTOR/ULK1 pathway could be reversed by applying mTOR activator, MHY1485. The results are shown in Fig. 7A–C and suggest that BNIP3 induced autophagy through the mTOR/ULK1 pathway in KGN cell.

Discussion

In this study, BNIP3 was identified as the hub molecule related to autophagy under hypoxia following OTT through bioinformatics analysis of GSE47555 from the GEO database. Subsequently, in vivo experiments showed that BNIP3 and autophagy were upregulated in primordial follicle GCs of mice early after OTT, which associated to cell death in GCs. Furthermore, BNIP3 was confirmed to activate autophagy via the mTOR/ULK1 pathway in the hypoxia-mimicking model of KGN cells induced by $CoCl_2$. According the results, it was hypothesized that BNIP3-media autophagy through mTOR/ULK1 was positively correlated with primordial follicle loss during

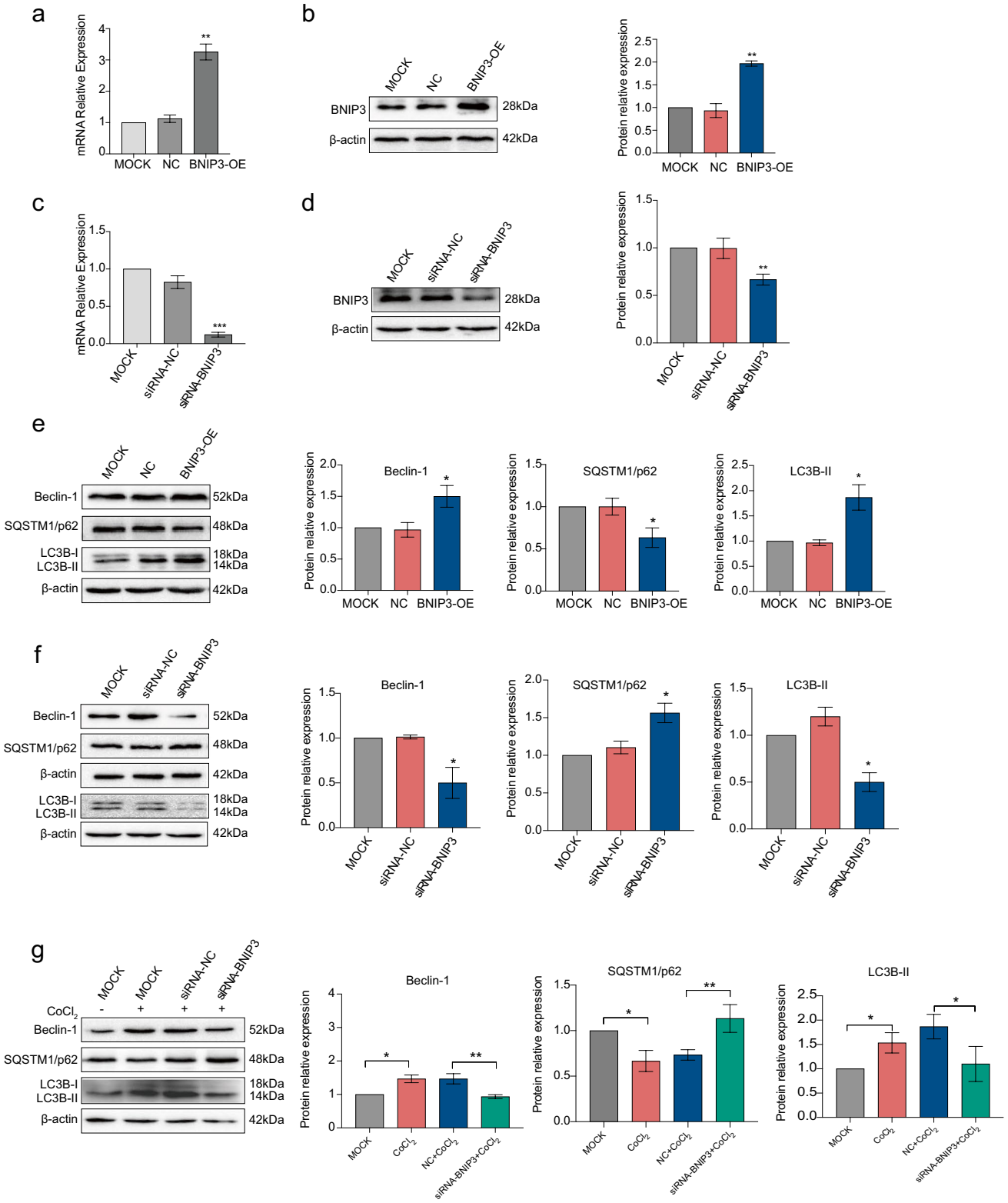

the OTT process, which proposes a novel explanation on the underlying mechanism and a therapeutic potential for resolving the clinical bottleneck of OTT.

OTT is an effective technology for preserving fertility, with restoration of endocrine function. In the OTT mice models, the re-activation of various stages of follicles was observed at 7 and 14 days after transplantation (Fig. S1),

◂**Fig. 6** BNIP3 induced autophagy in a hypoxia-mimicking model induced by $CoCl_2$. **a** qRT-PCR assay of KGN cells stably transfected with BNIP3 overexpression lentivirus. $^{**}P<0.01$. **b** Western blotting and quantitative assay of KGN cells stably transfected with BNIP3 overexpression lentivirus. **c** qRT-PCR assay of KGN cells stably transfected with BNIP3 shRNA lentivirus. $^{***}P<0.001$. **d** Western blotting and quantitative assay of KGN cells stably transfected with BNIP3 siRNA lentivirus. **e** Effect of BNIP3 overexpression on autophagy-associated protein expression in KGN cells based on western blotting analysis. **f** Effect of BNIP3 silencing on autophagy-associated protein expression in KGN cells based on western blotting analysis. **g** Effect of BNIP3 silencing on autophagy-associated protein expression in $CoCl_2$-treated KGN cells. $^{*}P<0.05$; $^{**}P<0.01$. OE overexpression, NC negative control

thus confirming the survival of ovarian tissue grafts and that OTT is an effective fertility preservation approach. However, the challenge of OTT with massive primordial follicle loss in the initial post transplantation period should not be ignored. The specific mechanisms of the phenomenon focused on are ischemic apoptosis and inappropriate follicle activation [29]. Only a few studies have linked autophagy to primordial follicle loss following OTT and hypothesize its key role during OTT procedure.

Autophagy promotes cell survival at the basal level by recycling energy and nutrients from abnormal cells and organelles, making it an essential physiological process for organismal homeostasis. In addition, abnormal autophagy could induce cell death, which may lead to a pathological state. Several studies have indicated that autophagy plays a major role in folliculogenesis and follicle atresia [30–33]. The mutation or knockout of ATG (ATG7, ATG9, and BECN1) leads to a reduction in ovarian reserve of adult mice [34, 35]. While activating the autophagy of newborn mice by specific autophagy-activator administration or starvation, the number of primordial follicles was increased accordingly [36, 37]. Another study reported that lack of lysine-specific demethylase 1 (LSD1) could induce excessive autophagy resulting in the autophagic death of oocyte, which suggested that autophagy contributed to the massive loss of follicles during the establishment of the primordial follicle pool [38]. Autophagy occurred primarily in ovarian GCs and contributed to follicle atresia, based on follicle analysis results at different stages [33]. Accordingly, autophagy appears to play a complex and dual role in follicle development. Although autophagy likely reacts to mild stimuli during the initial phase as a survival strategy, extensive and sustained autophagy triggers cell death pathways when stress persists and becomes severe. Amplified autophagy is closely associated with the death of GCs leading to follicular atresia, and hypoxia-induced autophagy in GCs is responsible at least in part for germ cell elimination of the mammalian ovary [33, 39]. The impacts of autophagy on ovary are diverse and complex. Autophagy is a pro-survival or pro-death mechanism, depending on ovarian cell type, follicle development stage, and stress condition [40]. Therefore, it is essential to distinguish cell types and follicle stages in order to evaluate the relationship between autophagy and follicle loss after OTT. The present study focused on autophagy activity change patterns in the GCs of primordial follicles with or without OTT.

Ovarian tissue perfusion after transplantation depends on neoangiogenic network formation rather than vascular anastomosis. Before the vascular network reconstruction, ovarian grafts are subjected to excessive hypoxic injury which may activate autophagy. The upregulated autophagy in GCs may be involved in primordial follicle loss, as the cross-talk between GCs and oocytes determines the outcome of follicles, and GCs are the primary site of hypoxia influence.

In our study, we screened BNIP3 as the hub gene during OTT process related to hypoxia and autophagy by bioinformatics analysis of GSE47555. All the experimental ovarian fragments of the GSE4775 dataset were also subjected to the freezing–thawing procedure. According to a previous study, the effect of ischemic injury on ovarian tissue following transplantation is more remarkable than freezing–thawing injury [41]. Therefore, we hypothesized that the major factor influencing gene expression patterns in the GSE4775 dataset was post-transplantation injury, and the hub gene BNIP3, may have a regulatory role in OTT.

The extensive reduction in primordial follicles was observed in mice on day 3 after transplantation, which is consistent with the findings of previous studies. TEM results showed that the accumulation of autophagic vacuoles occurred along with GCs death, which suggested the underlying association between autophagy and GCs death. Furthermore, the inhibition of autophagy by administration of 3-MA could significantly reverse primordial loss on day 3 after transplantation. These findings indicated that autophagy could promote primordial follicle loss during the OTT procedure in mice and that BNIP3 was correlated with the regulation.

As we screened BNIP3 as the hub gene in OTT procedure, we also explore the association between BNIP3 and primordial follicle loss by in vivo experiments. BNIP3 is an essential regulator of cellular response to hypoxia and is closely associated with hypoxia-related pathological changes and diseases including tumors and heart-brain ischemia injury [42]. Based on the analysis of different tumor and ischemia–reperfusion models, BNIP3 protein displays distinct expression patterns, suggesting the dual and intricate nature of BNIP3 regulation [43]. BNIP3 can either promote cell survival or cell death, and the regulation of cell fate (survival or death) by BNIP3 may be dependent on the specific context. BNIP3 is involved in hypoxia-dependent autophagic cell death [44]. Research also suggests that BNIP3 participates in folliculogenesis and follicle atresia, by inducing autophagy in hypoxia condition [45, 46].

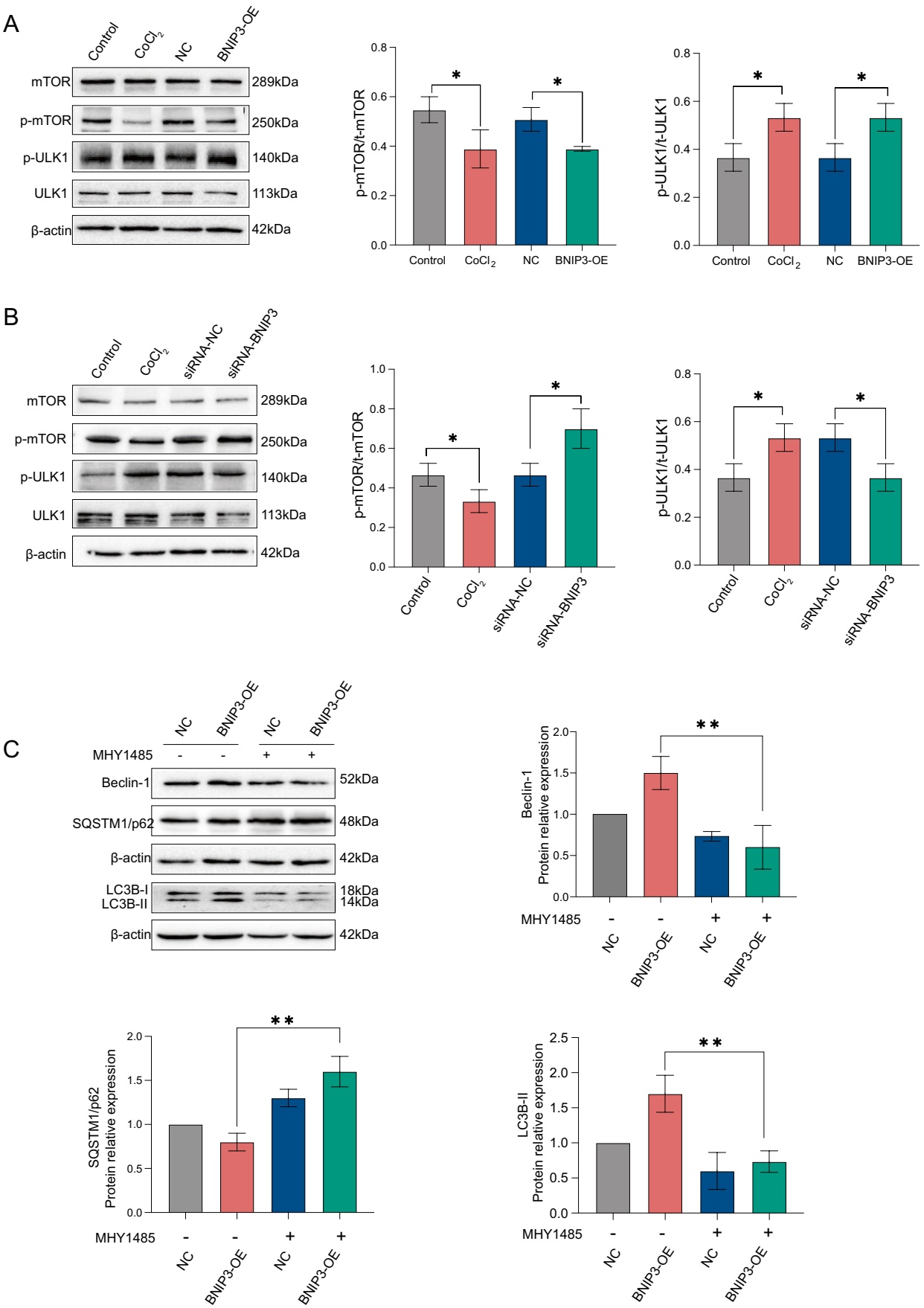
A
Control
CoCl2
NC
BNIP3-OE
mTOR
p-mTOR
p-ULK1
ULK1
β-actin
289kDa
250kDa
140kDa
113kDa
42kDa
p-mTOR/t-mTOR
p-ULK1/t-ULK1
B
siRNA-NC
siRNA-BNIP3
C
MHY1485
Beclin-1
SQSTM1/p62
LC3B-I
LC3B-II
52kDa
48kDa
18kDa
14kDa
Beclin-1 Protein relative expression
SQSTM1/p62 Protein relative expression
LC3B-II Protein relative expression

◂**Fig. 7** BNIP3 induced autophagy through the mTOR/ULK1 pathway. **A** Western blotting and the quantitative assay of the mTOR/ULK1 pathway after $CoCl_2$ treatment and BNIP3 overexpression. **B** Western blotting and the quantitative assay of the mTOR/ULK1 pathway after $CoCl_2$ treatment and BNIP3 silencing. **C** MHY1485 reversed autophagy activity induced by BNIP3 overexpression. Columns and bars represent the mean ± SD. $^*P < 0.05$; $^{**}P < 0.01$. OE overexpression, NC negative control, t-mTOR total mTOR protein, t-ULK1 total ULK1 protein

According to the protein expression data from Proteomicsdb database (https://www.proteomicsdb.org/) and IHC data from Human Protein Atlas database (https://www.proteinatlas.org/), BNIP3 is expressed ubiquitously in ovarian tissue rather than specifically in GCs. The IHC results of BNIP3 in our study were consistent with that. Since BNIP3 showed difference regulation mechanism in different cells, we analyzed the expression of BNIP3 in GCs of primordial follicles from fresh ovaries and ovarian grafts by quantitative analysis. We found that BNIP3 expression in GCs of primordial follicles increased along with autophagy activity after OTT at day 3, and the expression change was not affected by autophagy inhibitor 3-MA. The results suggested that BNIP3 may activate autophagy as an upstream molecule, and BNIP3 probably had an association with primordial follicle loss after OTT in mice.

Next, we further explored the regulation mechanism between BNIP3 and autophagy with in vitro experiments. $CoCl_2$ was applied to mimic hypoxia condition in KGN cells to further examine the details of how BNIP3 induced autophagy under hypoxia. The results showed that BNIP3 was upregulated both in mRNA and protein levels under hypoxia mimicking by $CoCl_2$, indicating that hypoxia contributes to the full expression of BNIP3 protein. In addition, the expression of autophagy-related protein (Beclin-1, LC3B, SQSTM1/p62), detection of autophagic vacuoles, and autophagy flux showed alterations along with hypoxia. These findings confirm that BNIP3 along with autophagy was activated by hypoxia. Furthermore, by detecting the protein level with western blot analysis in KGN cells, BNIP3 overexpression and silencing were found to promote and inhibit autophagy, respectively. Nevertheless, BNIP3-silencing reversed autophagy induced by $CoCl_2$. The above results indicated that hypoxia promoted BNIP3 activation, which then induced autophagy activation in KGN cells.

The mTOR/ULK1 pathway is a well-known regulator of autophagy in the initial stage [47]. The mTOR can be

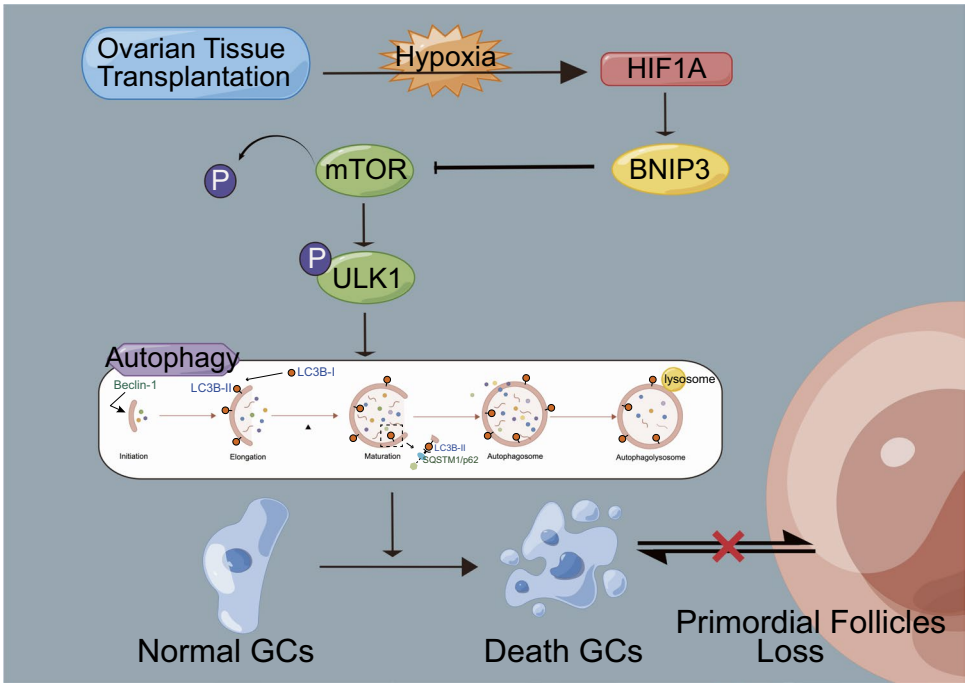

Fig. 8 Simplified schema graph showing possible mechanism of primordial follicles loss after ovarian tissue transplantation. Early after transplantation, ovarian tissue experiences a period of hypoxia with accumulation of HIF1A protein. BNIP3 is upregulated in hypoxia condition, which inhibits the mTOR and activates ULK1. The phosphorylation of ULK1 initiates autophagy process. Beclin-1, as an autophagy protein, is involved in the initiation and elongation stage of autophagy. LC3B-I converts to LC3B-II which binds to autophagosomal membranes. SQSTM1/p62 serves as a connection between LC3B-II and abnormal proteins and carries them to autophagosome. Autophagosome–lysosomes are fusions of lysosomes and autophagosomes and then degrade the contents. The activation of autophagy is along with the death of GCs and destroys the connection between GCs and oocytes resulting primordial follicles loss eventually. GCs granulosa cells

activated by phosphorylation in the normoxia environment. Once under the hypoxia condition, mTOR is inhibited by dephosphorylation and promotes downstream molecular ULK1 activation by phosphorylation, which triggers autophagy signaling cascades. The regulation of mTOR/ULK1 and autophagy in GCs has been reported before [48]. According to the results of our bioinformatics analysis, the mTOR pathway was enriched in the Top 20 of KEGG pathway enrichment results, which indicated that the mTOR pathway may play a role in OTT. In the present study, we introduce the mTOR/ULK1 pathway as an essential downstream regulator of autophagy induced by BNIP3. The expression of p-mTOR was inhibited while p-ULK1 was promoted following $CoCl_2$ treatment and BNIP3 overexpression in KGN cells. However, p-mTOR expression was enhanced while p-ULK1 was suspended following BNIP3 silencing. In addition, the administration of MHY1485, the mTOR activator, reversed the autophagy induced by BNIP3 overexpression. The results suggest that BNIP3 actives autophagy via the mTOR/ULK1 pathway in KGN cells.

The current study has limitations in that the experiments were performed in mice and cell line. It should be cautious to extrapolate these results to human ovarian tissue transplantation process. According to our findings, elucidating the exact role of BNIP3-media autophagy in primordial follicle loss after OTT continues to be a challenge, so that considerably more comprehensive investigations on the underlying mechanisms of the regulation of autophagy in ovarian grafts by BNIP3 are required.

Overall, our study demonstrates the activation of BNIP3 and autophagy activity in primordial follicle GCs of mice grafted ovaries in the hypoxia period, which may be the reason underlying the depletion of primordial follicles. In vitro experiments verified that BNIP3 promoted autophagy via the mTOR/ULK1 pathway under the hypoxia condition in KGN cells. Based on the findings, we proposed the mechanism underlying primordial follicle loss following OTT, as shown in Fig. 8, and illustrated using Figdraw (www.figdraw.com). The present study provides novel insights into the impact of BNIP3-media autophagy via mTOR/ULK1 pathway on primordial follicle loss after OTT, which may aid in the development of novel therapeutic targets to improve OTT outcomes.

Supplementary information The online version contains supplementary material available at https://doi.org/10.1007/s10815-023-02765-4.

Author contribution All the authors contributed to the study conception and design. Mujun Li supervised the study. Material preparation, data collection, and analysis were performed by Fengxia Liu. The first draft of the manuscript was written by Fengxia Liu, and all the authors commented on previous versions of the manuscript. All the authors read and approved the final manuscript.

Funding This research was funded by the Guangxi Key Research and Development Program, grant number AB20238002.

Data availability All data generated or analyzed during this study are included in this published article and its supplementary information files.

Declarations

Ethics approval Animal-based experiments were approved by the Animal Care & Welfare Committee of Guangxi Medical University (Approval Code: 202105009).

Consent Not applicable.

Competing interests The authors declare no competing interests.

References

1. Dolmans MM, Donnez J, Cacciottola L. Fertility preservation: the challenge of freezing and transplanting ovarian tissue. Trends Mol Med. 2021;27(8):777–91.
2. Oktay K, Harvey BE, Partridge AH, Quinn GP, Reinecke J, Taylor HS, Wallace WH, Wang ET, Loren AW. Fertility preservation in patients with cancer: ASCO clinical practice guideline update. J Clin Oncol. 2018;36(19):1994–2001.
3. Dolmans MM, von Wolff M, Poirot C, Diaz-Garcia C, Cacciottola L, Boissel N, Liebenthron J, Pellicer A, Donnez J, Andersen CY. Transplantation of cryopreserved ovarian tissue in a series of 285 women: a review of five leading European centers. Fertil Steril. 2021;115(5):1102–15.
4. Dolmans MM, Falcone T, Patrizio P. Importance of patient selection to analyze in vitro fertilization outcome with transplanted cryopreserved ovarian tissue. Fertil Steril. 2020;114(2):279–80.
5. Gavish Z, Spector I, Peer G, Schlatt S, Wistuba J, Roness H, Meirow D. Follicle activation is a significant and immediate cause of follicle loss after ovarian tissue transplantation. J Assist Reprod Genet. 2018;35(1):61–9.
6. Van Eyck AS, Jordan BF, Gallez B, Heilier JF, Van Langendonckt A, Donnez J. Electron paramagnetic resonance as a tool to evaluate human ovarian tissue reoxygenation after xenografting. Fertil Steril. 2009;92(1):374–81.
7. Fransolet M, Noël L, Henry L, Labied S, Blacher S, Nisolle M, Munaut C. Evaluation of Z-VAD-FMK as an anti-apoptotic drug to prevent granulosa cell apoptosis and follicular death after human ovarian tissue transplantation. J Assist Reprod Genet. 2019;36(2):349–59.
8. Lee S, Cho HW, Kim B, Lee JK, Kim T. The effectiveness of anti-apoptotic agents to preserve primordial follicles and prevent tissue damage during ovarian tissue cryopreservation and xenotransplantation. Int J Mol Sci. 2021;22(5):2534.
9. Wang HX, Lu XL, Huang WJ, Zhang JM. Pyroptosis is involved in cryopreservation and auto-transplantation of mouse ovarian tissues and pyroptosis inhibition improves ovarian graft function. Res Vet Sci. 2019;124:52–6.
10 Soleimani R, Heytens E, Oktay K. Enhancement of neoangiogenesis and follicle survival by sphingosine-1-phosphate in human ovarian tissue xenotransplants. Plos One. 2011;6(4):194.
11. D'Arcy MS. Cell death: a review of the major forms of apoptosis, necrosis and autophagy. Cell Biol Int. 2019;43(6):582–92.

12. Yang Y, Cheung HH, Law WN, Zhang C, Chan WY, Pei X, Wang Y. New insights into the role of autophagy in ovarian cryopreservation by vitrification. Biol Reprod. 2016;94(6):137.
13. Denton D, Kumar S. Autophagy-dependent cell death. Cell Death Differ. 2019;26(4):605–16.
14. Alers S, Löffler AS, Wesselborg S, Stork B. Role of AMPK-mTOR-Ulk1/2 in the regulation of autophagy: cross talk, shortcuts, and feedbacks. Mol Cell Biol. 2012;32(1):2–11.
15. Peters AE, Mihalas BP, Bromfield EG, Roman SD, Nixon B, Sutherland JM. Autophagy in female fertility: a role in oxidative stress and aging. Antioxid Redox Signal. 2020;32(8):550–68.
16. Gilchrist RB, Lane M, Thompson JG. Oocyte-secreted factors: regulators of cumulus cell function and oocyte quality. Hum Reprod Update. 2008;14(2):159–77.
17. Xu Z. Autophagy phenomenon in mice ovaries following transplantation. Theriogenology. 2023;195:40–5.
18. Guo Z, Tang N, Liu FY, Yang Z, Ma SQ, An P, Wu HM, Fan D, Tang QZ. TLR9 deficiency alleviates doxorubicin-induced cardiotoxicity via the regulation of autophagy. J Cell Mol Med. 2020;24(18):10913–23.
19. Yan Z, Li Q, Zhang L, Kang B, Fan W, Deng T, Zhu J, Wang Y. The growth and development conditions in mouse offspring derived from ovarian tissue cryopreservation and orthotopic transplantation. J Assist Reprod Genet. 2020;37(4):923–32.
20. Scudamore CL. A practical guide to the histology of the mouse. In: Scudamore CL, editor. Reproductive system. UK: Wiley; 2014. p. 89–91.
21. Muñoz-Sánchez J, Chánez-Cárdenas ME. The use of cobalt chloride as a chemical hypoxia model. J Appl Toxicol. 2019;39(4):556–70.
22. Wu Y, Ma C, Zhao H, Zhou Y, Chen Z, Wang L. Alleviation of endoplasmic reticulum stress protects against cisplatin-induced ovarian damage. Reprod Biol Endocrinol. 2018;16(1):85.
23. Wang L, Hao H, Wang J, Wang X, Zhang S, Du Y, Lv T, Zuo L, Li Y, Liu H. Decreased autophagy: a major factor for cardiomyocyte death induced by β1-adrenoceptor autoantibodies. Cell Death Dis. 2015;6(8):e1862.
24. Mizushima N, Yoshimori T, Levine B. Methods in mammalian autophagy research. Cell. 2010;140(3):313–26.
25. Nishi Y, Yanase T, Mu Y, Oba K, Ichino I, Saito M, Nomura M, Mukasa C, Okabe T, Goto K, Takayanagi R, Kashimura Y, Haji M, Nawata H. Establishment and characterization of a steroidogenic human granulosa-like tumor cell line, KGN, that expresses functional follicle-stimulating hormone receptor. Endocrinology. 2001;142(1):437–45.
26. Zhou XY, Zhang J, Li Y, Chen YX, Wu XM, Li X, Zhang XF, Ma LZ, Yang YZ, Zheng KM, Liu YD, Wang Z, Chen SL. Advanced oxidation protein products induce G1/G0-phase arrest in ovarian granulosa cells via the ROS-JNK/p38 MAPK-p21 pathway in premature ovarian insufficiency. Oxid Med Cell Longev. 2021;2021:6634718.
27. Yi S, Zheng B, Zhu Y, Cai Y, Sun H, Zhou J. Melatonin ameliorates excessive PINK1/Parkin-mediated mitophagy by enhancing SIRT1 expression in granulosa cells of PCOS. Am J Physiol Endocrinol Metab. 2020;319(1):E91-e101.
28. Zhu F, Gao J, Zeng F, Lai Y, Ruan X, Deng G. Hyperoside protects against cyclophosphamide induced ovarian damage and reduced fertility by suppressing HIF-1α/BNIP3-mediated autophagy. Biomed Pharmacother. 2022;156: 113743.
29. Liu J, Van der Elst J, Van den Broecke R, Dhont M. Early massive follicle loss and apoptosis in heterotopically grafted newborn mouse ovaries. Hum Reprod. 2002;17(3):605–11.
30. Zhou J, Peng X, Mei S. Autophagy in ovarian follicular development and atresia. Int J Biol Sci. 2019;15(4):726–37.
31. Zheng Y, Ma L, Liu N, Tang X, Guo S, Zhang B, Jiang Z. Autophagy and apoptosis of porcine ovarian granulosa cells during follicular development. Animals (Basel). 2019;9(12):111.
32. Leopardo NP, Velazquez ME, Cortasa S, González CR, Vitullo AD. A dual death/survival role of autophagy in the adult ovary of Lagostomus maximus (Mammalia- Rodentia). PLoS ONE. 2020;15(5): e0232819.
33. Choi JY, Jo MW, Lee EY, Yoon BK, Choi DS. The role of autophagy in follicular development and atresia in rat granulosa cells. Fertil Steril. 2010;93(8):2532–7.
34. Delcour C, Amazit L, Patino LC, Magnin F, Fagart J, Delemer B, Young J, Laissue P, Binart N, Beau I. ATG7 and ATG9A loss-of-function variants trigger autophagy impairment and ovarian failure. Genet Med. 2019;21(4):930–8.
35. Gawriluk TR, Hale AN, Flaws JA, Dillon CP, Green DR, Rucker EB 3rd. Autophagy is a cell survival program for female germ cells in the murine ovary. Reproduction. 2011;141(6):759–65.
36. Watanabe R, Kimura N. Non-suckling starvation of neonatal mice promotes primordial follicle formation with activation of ovarian autophagy. J Reprod Dev. 2018;64(1):89–94.
37. Watanabe R, Sasaki S, Kimura N. Activation of autophagy in early neonatal mice increases primordial follicle number and improves lifelong fertility†. Biol Reprod. 2020;102(2):399–411.
38. He M, Zhang T, Zhu Z, Qin S, Wang H, Zhao L, Zhang X, Hu J, Wen J, Cai H, Xin Q, Guo Q, Lin L, Zhou B, Zhang H, Xia G, Wang C. LSD1 contributes to programmed oocyte death by regulating the transcription of autophagy adaptor SQSTM1/p62. Aging Cell. 2020;19(3): e13102.
39. Yadav AK, Yadav PK, Chaudhary GR, Tiwari M, Gupta A, Sharma A, Pandey AN, Pandey AK, Chaube SK. Autophagy in hypoxic ovary. Cell Mol Life Sci. 2019;76(17):3311–22.
40. Bhardwaj JK, Paliwal A, Saraf P, Sachdeva SN. Role of autophagy in follicular development and maintenance of primordial follicular pool in the ovary. J Cell Physiol. 2022;237(2):1157–70.
41. Lee J, Kong HS, Kim EJ, Youm HW, Lee JR, Suh CS, Kim SH. Ovarian injury during cryopreservation and transplantation in mice: a comparative study between cryoinjury and ischemic injury. Hum Reprod. 2016;31(8):1827–37.
42. Zhang J, Ney PA. Role of BNIP3 and NIX in cell death, autophagy, and mitophagy. Cell Death Differ. 2009;16(7):939–46.
43 Gorbunova AS, Yapryntseva MA, Denisenko TV, Zhivotovsky B. BNIP3 in lung cancer: to kill or rescue? Cancers (Basel). 2020;12(11):339.
44. Bellot G, Garcia-Medina R, Gounon P, Chiche J, Roux D, Pouysségur J, Mazure NM. Hypoxia-induced autophagy is mediated through hypoxia-inducible factor induction of BNIP3 and BNIP3L via their BH3 domains. Mol Cell Biol. 2009;29(10):2570–81.
45. Tang Z, Xu R, Zhang Z, Shi C, Zhang Y, Yang H, Lin Q, Liu Y, Lin F, Geng B, Wang Z. HIF-1α protects granulosa cells from hypoxia-induced apoptosis during follicular development by inducing autophagy. Front Cell Dev Biol. 2021;9: 631016.
46. Zhou J, Yao W, Li C, Wu W, Li Q, Liu H. Administration of follicle-stimulating hormone induces autophagy via upregulation of HIF-1α in mouse granulosa cells. Cell Death Dis. 2017;8(8):e3001.
47. Kim J, Kundu M, Viollet B, Guan KL. AMPK and mTOR regulate autophagy through direct phosphorylation of Ulk1. Nat Cell Biol. 2011;13(2):132–41.
48. Lin M, Hua R, Ma J, Zhou Y, Li P, Xu X, Yu Z, Quan S. Bisphenol A promotes autophagy in ovarian granulosa cells by inducing

AMPK/mTOR/ULK1 signalling pathway. Environ Int. 2021;147: 106298.